Research Article | Vol. 30, No. 2 / 17 Jan 2022 / Optics Express 1664

Optics EXPRESS

Explanation of the anomalous redshift on a nonlinear X-ray Compton scattering spectrum by a bound electron

SHANG SHI,[1,2] JING CHEN,[3,4] YUJUN YANG,[5] ZHONG-CHAO YAN,[6,7] XIAOJUN LIU,[7] AND BINGBING WANG[1,2,*]

[1]*Laboratory of Optical Physics, Beijing National Laboratory for Condensed Matter Physics, Institute of Physics, Chinese Academy of Sciences, Beijing 100190, China*
[2]*University of Chinese Academy of Sciences, Beijing 100049, China*
[3]*HEDPS, Center for Applied Physics and Technology, Peking University, Beijing 100871, China*
[4]*Institute of Applied Physics and Computational Mathematics, Beijing 100088, China*
[5]*Insititute of Atomic and Molecular Physics, Jilin University, Changchun 130012, China*
[6]*Department of Physics, University of New Brunswick, Fredericton, New Brunswick E3B 5A3, Canada*
[7]*State Key Laboratory of Magnetic Resonance and Atomic and Molecular Physics, Wuhan Institute of Physics and Mathematics, Innovation Academy for Precision Measurement Science and Technology, Chinese Academy of Sciences, Wuhan 430071, China*
[*]*wbb@aphy.iphy.ac.cn*

Abstract: Nonlinear Compton scattering is an inelastic scattering process where a photon is emitted due to the interaction between an electron and an intense laser field. With the development of X-ray free-electron lasers, the intensity of X-ray laser is greatly enhanced, and the signal from X-ray nonlinear Compton scattering is no longer weak. Although the nonlinear Compton scattering by an initially free electron has been thoroughly investigated, the mechanism of nonrelativistic nonlinear Compton scattering of X-ray photons by bound electrons is unclear yet. Here, we present a frequency-domain formulation based on the nonperturbative quantum electrodynamics to study nonlinear Compton scattering of two photons by an atom in a strong X-ray laser field. In contrast to previous theoretical works, our results clearly reveal the existence of a redshift phenomenon observed experimentally by Fuchs *et al.* (Nat. Phys.)**11**, 964(2015) and suggest its origin as the binding energy of the electron as well as the momentum transfer from incident photons to the electron during the scattering process. Our work builds a bridge between intense-laser atomic physics and Compton scattering processes that can be used to study atomic structure and dynamics at high laser intensities.

1. Introduction

The Compton effect is well known for proving the quantum hypothesis of light in 1923 experimentally [1]. Afterwards the impulse approximation (IA) approach to Compton scattering on bound electrons, which considers the initial electron to be free with the momentum distribution of the bound state, was put forward by DuMond in his work on the scattering of photons from solids [2,3]. Since the Compton profile is directly related to the electron momentum distribution, the electronic structure of atoms, molecules and solids can be probed by X- and γ-ray linear Compton scattering (LCS) [4–7] and analyzed by IA. For LCS process, Eisenberger and Platzman verified the validity of nonrelativistic IA for doubly differential cross sections [8], and later Ribberfors extended IA to relativistic region [9]. Modification of IA and reexamination of the validity of IA have been the main interests of recent studies [10–12].

With the first use of the Linac Coherent Light Source at the SLAC National Accelerator Laboratory in 2009 [13], the era of exploring the nonlinear interaction of ultrafast and ultra-intense X-rays with matters has begun. By using X-ray free-electron lasers [14–17], people have observed

#448633 https://doi.org/10.1364/OE.448633
Journal © 2022 Received 15 Nov 2021; accepted 6 Dec 2021; published 5 Jan 2022

Optics EXPRESS

for the first time extensive nonlinear phenomena at X-ray wavelengths, including the X-ray second harmonic generation in diamonds [18], two-photon absorption in the hard X-ray region [19,20], electron femtosecond response to an ultra-intense X-ray radiation [21], and nonlinear Compton scattering (NCS) of X-ray photons [22]. Among them, the NCS is a particularly interesting phenomenon because the observed anomalous redshift of the scattered photon can be regarded as a breakdown of the widely-used IA theory for bound electrons.

There exist a few theoretical studies [23–25] devoted to the NCS processes involving bound electrons in recent years, but no theoretical work demonstrated the experimental observations by Fuchs *et al.* [22]. For example, Krebs *et al.* [24] developed a nonperturbative approach based on the time-dependent Schrödinger equation to investigate linear and nonlinear Compton scatterings of X-ray photons by atoms. However, their results were consistent with the predictions of the free-electron model and do not support the existence of the redshift found in Ref. [22]. More recently, Venkatesh and Robicheaux [25] claimed that their theoretical results exhibit a blueshift compared with the scattered photon energy predicted by the free-electron model during an NCS process. Therefore, the origin of the anomalous redshift phenomenon observed by Fuchs *et al.* [22] is still an open question.

Motivated by the theoretical gap of the NCS mechanism, in this work we will apply the frequency-domain theory based on the nonperturbative quantum electrodynamics (QED) to study the NCS processes of bound electrons. This theory has previously been successfully applied in investigating recollision processes in strong laser fields [26–29]. The advantages of the QED method in treating the NCS could be shortly provided. Specifically, we will focus on the double differential probability (DDP) of a NCS process by a bound electron in an X-ray laser field. Our calculation will clearly demonstrate that in the DDP spectrum of the two-photon NCS, as the energy of the scattered photon increases, a redshift peak will appear, which agrees with the observation by Fuchs *et al.* [22] qualitatively.

2. Frequency-domain theory of the NCS by bound electrons

In the frequency-domain theory based on the QED, the whole system consists of an atom and radiation fields, where the radiation fields are linearly polarized and quantized, involving incident and scattered photons in Compton scattering processes. In the following, natural units ($\hbar = m = c = 1$) are used throughout unless otherwise stated, where m is the electron rest mass and c the speed of light. The Hamiltonian of this atom-radiation system is

$$H = H_0 + U + V, \tag{1}$$

where

$$H_0 = \frac{(-i\nabla)^2}{2} + \omega_1 N_{a_1} + \omega_2 N_{a_2} \tag{2}$$

is the non-interaction part of the Hamiltonian, with $N_{a_1} = (a_1^\dagger a_1 + a_1 a_1^\dagger)/2$ and $N_{a_2} = (a_2^\dagger a_2 + a_2 a_2^\dagger)/2$ being the number operators of the incident and the scattered photons, respectively, with $a_i(a_i^\dagger)$ being the annihilation (creation) operator for $i = 1, 2$, and ω_1 is the incident laser frequency and ω_2 the scattered photon frequency. U is the atomic binding potential, and V is the total electron-photon interaction potential that can be written as $V = V_1 + V_{21} + V_{22}$ with

$$V_1 = e\mathbf{A}_1(\mathbf{r}) \cdot (-i\nabla) + \frac{e^2\mathbf{A}_1^2(\mathbf{r})}{2}, \tag{3}$$

$$V_{21} = e^2\mathbf{A}_1(\mathbf{r}) \cdot \mathbf{A}_2(\mathbf{r}), \tag{4}$$

and

$$V_{22} = e\mathbf{A}_2(\mathbf{r}) \cdot (-i\nabla), \tag{5}$$

Optics EXPRESS

where e is the elementary charge. Here, we have neglected the term $\frac{e^2\mathbf{A}_2^2(\mathbf{r})}{2}$ for its weak strength compared with the above three terms V_1, V_{21} and V_{22}. The vector potentials of the incident and scattered photon modes are $\mathbf{A}_1(\mathbf{r}) = g_1(\boldsymbol{\epsilon}_1 a_1 e^{i\mathbf{k}_1\cdot\mathbf{r}} + \text{c.c.})$ and $\mathbf{A}_2(\mathbf{r}) = g_2(\boldsymbol{\epsilon}_2 a_2 e^{i\mathbf{k}_2\cdot\mathbf{r}} + \text{c.c.})$, where $\mathbf{r}$ is the spatial coordinate of the electron. $g_1 = (2\omega_1 V_\gamma)^{\frac{-1}{2}}$ and $g_2 = (2\omega_2 V'_\gamma)^{\frac{-1}{2}}$ with V_γ and V'_γ the normalization volumes of the photon modes, $\mathbf{k}_1$ ($\mathbf{k}_2$) and $\boldsymbol{\epsilon}_1$ ($\boldsymbol{\epsilon}_2$) are the wave vector and polarization vector of the incident laser field (scattered photon mode), respectively. By substituting the expressions of $\mathbf{A}_1(\mathbf{r})$ and $\mathbf{A}_2(\mathbf{r})$ into Eq. (4) and Eq. (5), we obtain the explicit expressions of V_{21} and V_{22}, where V_{21} can be split into two terms

$$V_{21-} = e^2 g_1 g_2 \boldsymbol{\epsilon}_2^* \cdot \boldsymbol{\epsilon}_1 e^{i(\mathbf{k}_1-\mathbf{k}_2)\cdot\mathbf{r}} a_1 a_2^\dagger, \tag{6}$$

and

$$V_{21+} = e^2 g_1 g_2 \boldsymbol{\epsilon}_2^* \cdot \boldsymbol{\epsilon}_1^* e^{-i(\mathbf{k}_1+\mathbf{k}_2)\cdot\mathbf{r}} a_1^\dagger a_2^\dagger, \tag{7}$$

and V_{22} can be written as

$$V_{22} = e g_2 e^{-i\mathbf{k}_2\cdot\mathbf{r}} a_2^\dagger \boldsymbol{\epsilon}_2^* \cdot (-i\nabla). \tag{8}$$

Here, the terms containing the annihilation operator a_2, which make no contribution to NCS processes, are not included in Eq. (6)-(8).

Since the atom-radiation system can be regarded as an isolated one, the total energy of the system is conserved during the atom-radiation interaction process and the formal scattering theory [30] can be applied. The scattering matrix (S-matrix) element [27,28] is expressed as

$$S_{fi} = \langle \psi_f^- | \psi_i^+ \rangle, \tag{9}$$

where

$$\psi_j^\pm = \psi_j + \frac{1}{E_j - H \pm i\varepsilon} V\psi_j \tag{10}$$

with j taken to be i or f and ε to be a small positive real number. Physically, ψ_i^+ is the scattering state at $t = 0$ which has developed from a pre-collision state ψ_i in the remote past, whereas ψ_f^- is the scattering state at $t = 0$ which will develop to a post-collision state ψ_f in the remote future. After some algebraic manipulation, the S-matrix element can be recast into

$$S_{fi} = \delta_{fi} - 2\pi i \delta(E_f - E_i) T_{fi}, \tag{11}$$

where T_{fi} is the exact transition matrix (T-matrix) element [31,32] between the initial state $|\psi_i\rangle$ and the final state $|\psi_f\rangle$, and can be written as

$$T_{fi} = \langle \psi_f | U | \psi_i^+ \rangle. \tag{12}$$

Substituting Eq. (10) into Eq. (12), we have

$$T_{fi} = \langle \psi_f | V | \psi_i \rangle + \langle \psi_f | V \frac{1}{E_i - H + i\varepsilon} V | \psi_i \rangle. \tag{13}$$

Here, the initial state $|\psi_i\rangle = \Phi_i(\mathbf{r}) \otimes |l\rangle \otimes |0\rangle$ is the eigenstate of the operator $H_0 + U$ with the eigenenergy $E_i = (-E_B) + (l + \frac{1}{2})\omega_1 + \frac{1}{2}\omega_2$. $\Phi_i(\mathbf{r})$ is the ground-state wave function of the electron in an atom with the binding energy E_B>0, and $|l\rangle$ and $|0\rangle$ are the Fock states of the incident and scattered photons with photon number l and 0, respectively. The final state $|\psi_f\rangle = \Psi_{\mathbf{P}_f n_f} \otimes |1\rangle$ is the eigenstate of the operator $H_0 + V$ with the eigenenergy $E_f = \mathbf{P}_f^2/2 + (n_f + \frac{1}{2} + u_p)\omega_1 + \frac{3}{2}\omega_2$, where $\mathbf{P}_f$ is the final momentum of the electron, n_f is the laser photon number of the final state

Optics EXPRESS

and u_p the ponderomotive energy in unit of the incident photon energy. $\Psi_{\mathbf{P}_f n_f}$ is the Volkov state of the electron in the laser field [26]

$$\Psi_{\mathbf{P}_f n_f} = V_e^{-1/2} \sum_{n=-n_f}^{\infty} e^{i[\mathbf{P}_f + (u_p - n)\mathbf{k}_1]\cdot \mathbf{r}} \mathcal{J}_n(\zeta, \eta)^* |n_f + n\rangle. \tag{14}$$

In the above, V_e is the normalization volume of the final momentum of the electron, $\mathcal{J}_n(\zeta, \eta) = \sum_{s=-\infty}^{\infty} J_{-n-2s}(\zeta) J_s(\eta)$ is the generalized Bessel function with the arguments $\zeta = 2\sqrt{\frac{u_p}{\omega_1}} \mathbf{P}_f \cdot \boldsymbol{\epsilon}_1$ and $\eta = u_p/2$, the subscript n represents the number of transferred photons and s is an integer.

The first and second terms in Eq. (13) correspond to one-step and two-step transitions, respectively. In order to compare with the experimental results [22], we focus on peak positions of the DDP spectra in this work, where there is no contribution from the two-step transition under the laser condition of laser intensity being $4 \times 10^{20}\,\mathrm{W/cm}^2$ with photon energy ω_1=9.25 keV, hence the second term in Eq. (13) is dropped and will be investigated in the future. Therefore, the T-matrix element for NCS can be expressed as

$$T_{fi} = T_{AA-} + T_{AA+} + T_{AP}, \tag{15}$$

where the matrix elements of the EMM transitions $T_{AA\pm}$ are given by

$$\begin{aligned} T_{AA-} &= \langle \psi_f | V_{21-} | \psi_i \rangle \\ &= e^2 V_e^{-1/2} \Lambda g_2 \boldsymbol{\epsilon}_1 \cdot \boldsymbol{\epsilon}_2^* \mathcal{J}_{q-1}(\zeta, \eta) \Phi_i(\mathbf{P}_f + \mathbf{k}_2 + (u_p - q)\mathbf{k}_1) \end{aligned} \tag{16}$$

and

$$\begin{aligned} T_{AA+} &= \langle \psi_f | V_{21+} | \psi_i \rangle \\ &= e^2 V_e^{-1/2} \Lambda g_2 \boldsymbol{\epsilon}_1^* \cdot \boldsymbol{\epsilon}_2^* \mathcal{J}_{q+1}(\zeta, \eta) \Phi_i(\mathbf{P}_f + \mathbf{k}_2 + (u_p - q)\mathbf{k}_1), \end{aligned} \tag{17}$$

where $\Lambda = \sqrt{\frac{u_p \omega_1}{\alpha}}$ with α being the fine-structure constant [33,34], and $q = l - n_f$ denotes the number of photons transferred from the incident laser field during the NCS process. And the matrix element of the LEM transition T_{AP} can be written as

$$\begin{aligned} T_{AP} &= \langle \psi_f | V_{22} | \psi_i \rangle \\ &= e V_e^{-1/2} g_2 \boldsymbol{\epsilon}_2^* \cdot [\mathbf{P}_f + (u_p - q)\mathbf{k}_1] \mathcal{J}_q(\zeta, \eta) \Phi_i(\mathbf{P}_f + \mathbf{k}_2 + (u_p - q)\mathbf{k}_1). \end{aligned} \tag{18}$$

In Eq. (16)–(18), the two-photon NCS processes correspond to $q = 2$.

Figure 1 illustrates the corresponding schematic diagrams of the three terms in Eq. (15), where we name T_{AP} the laser-assisted electron-mode (LEM) transition shown in Fig. 1(a), and name T_{AA-} and T_{AA+} the electron-assisted mode-mode (EMM) transitions shown in Fig. 1(b) and (c) respectively. The LEM transition describes the process where the bound electron is ionized after absorbing several photons from the laser field, and at the same time, a photon of frequency ω_2 is scattered, whereas the EMM transition describes a similar process except that a second photon of frequency ω_1 is either absorbed (T_{AA-}) or emitted (T_{AA+}).

The expression of the DDP for a Compton scattering process can be written as

$$\frac{dW_{i\to f}}{d\omega_2 d\Omega} = \int 2\pi |T_{fi}|^2 \delta(E_i - E_f) \frac{V_{\gamma_2}}{(2\pi)^3} \frac{V_e}{(2\pi)^3} \omega_2^2 d^3 P_f, \tag{19}$$

where $d\Omega$ is the differential solid angle of vector $\mathbf{k}_2$. To analyze the results more clearly, we may rewrite the DDP by three parts:

$$\frac{dW_{i\to f}}{d\omega_2 d\Omega} = \frac{dW_{AP}}{d\omega_2 d\Omega} + \frac{dW_{AA}}{d\omega_2 d\Omega} + \frac{dW_{CT}}{d\omega_2 d\Omega}, \tag{20}$$

where the three parts on the right-hand of the equation represent the contributions of EMM, LEM and their cross term (CT). In the following, we will see how these terms affect the peak position of the DDP spectrum of two-photon NCS processes.

Optics EXPRESS

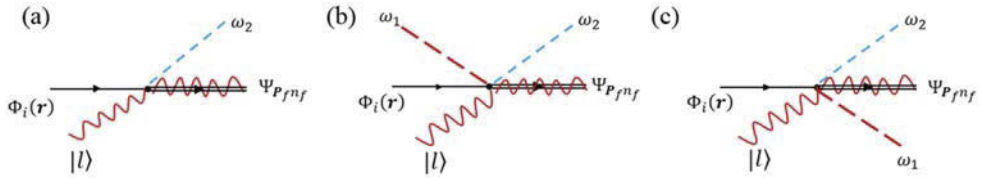

Fig. 1. Schematic for the one-step transition of the NCS by a bound electron. The single straight line represents the bound electron state, the wavy line represents the Fock state of the incident laser, the combination of wavy and double lines represents the Volkov state, the red and blue dashed lines represent the scattered photons of frequency ω_1 and ω_2 respectively, and the vertex denotes the transition operator V_{22} in (**a**), V_{21-} in (**b**), and V_{21+} in (**c**).

3. Redshift

According to the experimental set-up in Ref. [22], the polarization and wave vectors of the incident laser field are chosen along the x- and z-axis, respectively, while the direction of $\mathbf{k}_2$ is characterized by the spherical coordinates (θ, ϕ), as shown in Fig. 2. Since the polarization direction of the scattered light is not fixed in Ref. [22], we integrate all the polarization directions of the scattered light in our calculation.

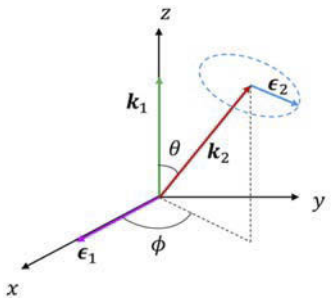

Fig. 2. Geometry of the NCS for initially linearly polarized light. The polarization and wave vectors of the incoming photons define the xz plane, while the direction of the scattered photons is characterized by the spherical coordinates (θ, ϕ).

We now calculate the DDP for Compton scattering of two X-ray laser photons by a $1s$ electron of Be atom, where the intensity of the incident laser field is 4×10^{20} W/cm^2 with the photon energy of 9.25 keV. In order to compare the DDP spectra with those of the experiment by Fuchs *et al.*, the wave vector of the scattered photon $\mathbf{k}_2$ is fixed in the polarization plane of the incident laser field defined by $\mathbf{k}_1$ (z-axis) and $\boldsymbol{\epsilon}_1$ (x-axis), i.e., the azimuthal angle $\phi = 0°$. The DDP of the NCS at the scattering angles of $\theta = 89°$ (a), $103°$ (b), $117°$ (c) and $131°$ (d) are displayed by solid lines in Fig. 3. The vertical lines indicate the scattered photon energy predicted by the free-electron model [24,25,35]:

$$\omega_2 = \frac{q\omega_1}{1 + q\omega_1(1 - \cos\theta)}, \tag{21}$$

It can be seen from Fig. 3 that the peak positions in the scattered spectra for the four angles are all red shifted to the scattered photon energy predicted by the free-electron model, which qualitatively agrees with the experimental observations [22].

In order to explain the results shown in Fig. 3, we present separately the contributions to the total DDP by tranistions T_{AP} (short-dotted lines), T_{AA-} (dash-dotted lines) and T_{AA+} (short-dashed lines) as well as the cross term (dashed lines) in Fig. 3(a)-(d). One can see that the contribution

Optics EXPRESS

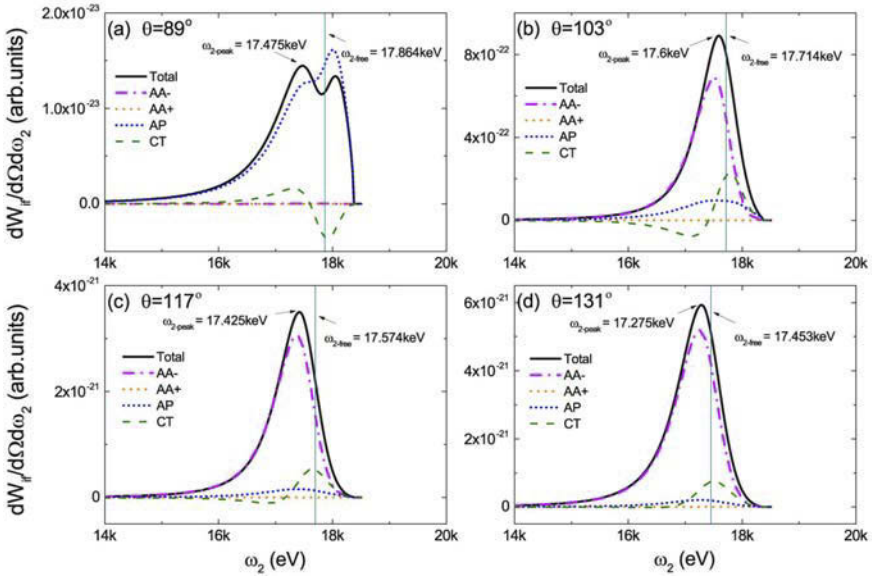

Fig. 3. The DDP as a function of the scattered photon energy ω_2 at the scattering angle of $\theta = 89°$ (**a**), $\theta = 103°$ (**b**) , $\theta = 117°$ (**c**) and $\theta = 131°$ (**d**). The solid lines represent the total DDP. The short-dotted lines, dash-dotted lines, and short-dashed lines represent the DDP determined by T-matrix elements T_{AP}, T_{AA-} and T_{AA+}. The dashed lines show the distribution of the cross term (CT). The vertical lines are ω_2 predicted by Eq. (19). The scattered wave vector $\mathbf{k}_2$ is fixed in the polarization plane defined by $\mathbf{k}_1$ and $\boldsymbol{\epsilon}_1$. The incident X-ray laser intensity is 4×10^{20} W/cm^2 with photon energy of 9.25 keV.

of T_{AA+} can be ignored, hence the EMM transition mentioned below refers to the T_{AA-} transition. For $\theta = 89°$, although the total DDP is dominated by the LEM transition which is blue shifted to the energy predicted by the free-electron model, the contribution from the cross term plays a crucial role in the DDP spectrum, where it increases the probability in lower energy region and decreases the probability in higher energy region. Thus, a bimodal structure with higher peak in lower energy of the spectrum appears. For $\theta = 103°, 117°$ and $131°$, since the total DDP is dominated by EMM transition, the peak positions of total DDP spectra are all redshifted to the energy predicted by the free-electron model.

Furthermore, Fig. 3 shows that the peak positions of the DDP spectrum by EMM transition are always red shifted to the energy given by the free-electron model, while the peak positions of that by LEM transition can be either blue shifted or red shifted. To find the reason of these calculation results, we simplify Eq. (16) and Eq. (18) by replacing the generalized Bessel functions $\mathcal{J}_1(\zeta, \eta)$ with $J_{-1}(\zeta) \approx C_1 \mathbf{P}_f \cdot \boldsymbol{\epsilon}_1$ and $\mathcal{J}_2(\zeta, \eta)$ with $J_{-1}(\eta) + J_{-2}(\zeta) \approx C_2$, as the values of ζ and η are much smaller than 1 under the present laser conditions ($|\zeta|$<0.034, $\eta = 3.6 \times 10^{-5}$). Here the parameters C_1 and C_2 are constants determined by the laser conditions. Therefore, the matrix element of EMM transition can be approximated as

$$T_{AA-} \approx e^2 V_e^{-1/2} \Lambda g_2 C_1 \boldsymbol{\epsilon}_1 \cdot \boldsymbol{\epsilon}_2^* P_f \cos\theta_{\epsilon_1} \Phi_i(\mathbf{P}_f + \mathbf{k}_2 - q\mathbf{k}_1) \tag{22}$$

with θ_{ϵ_1} being the angle between $\boldsymbol{\epsilon}_1$ and the electron momentum $\mathbf{P}_f$. And the matrix element of LEM transition can be approximated as

$$T_{AP} \approx -eV_e^{-1/2} g_2 C_2 (P_f \cos\theta_{\epsilon_2} - q\mathbf{k}_1 \cdot \boldsymbol{\epsilon}_2^*) \Phi_i(\mathbf{P}_f + \mathbf{k}_2 - q\mathbf{k}_1) \tag{23}$$

Optics EXPRESS

with θ_{ϵ_2} being the angle between $\boldsymbol{\epsilon}_2^*$ and the electron momentum $\mathbf{P}_f$. The DDP spectra by Eq. (22) (olive short-dotted lines) and by Eq. (23) (magenta dotted lines) are shown in Fig. 4(a)-(b), consistent with the results by Eq. (16) and Eq. (18), respectively.

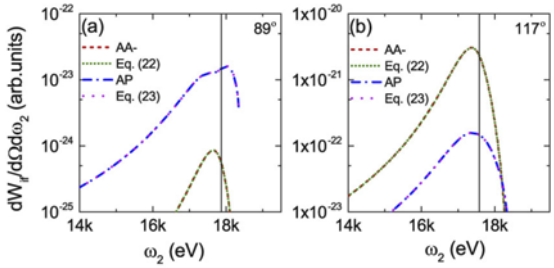

Fig. 4. The DDP by the T-matrix element T_{AA-} (red short-dashed lines) and the DDP by Eq. (22) (olive short-dotted lines), and the DDP by the T-matrix element T_{AP} (blue dash-dotted lines) and the DDP by Eq. (23) (magenta dotted lines) at $\theta = 89°$ (**a**) and $\theta = 117°$ (**b**). The laser parameters and azimuthal angle of the scattered wave vector are the same as Fig. 3.

We firstly consider the influence of the atomic wavefunction on the DDP spectra, which is contained in Eq. (22)-(23). By integrating the modular square of the wavefunction over $\mathbf{P}_f$, we obtain the electron density distribution as a function of the scattered photon energy ω_2 and the scattering angle θ, as shown in Fig. 5. It shows that the peak positions presented by dots on the density distribution decrease with the scattering angle. This can be explained as follows: By analyzing the argument of the wavefunction, it can be found that the peak of the electron density distribution occurs at the momentum transfer $\mathbf{P}_f = q\mathbf{k}_1 - \mathbf{k}_2$, as illustrated by the inset of Fig. 5. Since this momentum transfer increases with the scattering angle, the energy gained by electron from the scattering process increase inevitably, leading to a decrease of the scattered photon energy. Moreover, one may find that the peaks of the density distribution are always redshifted to the prediction of the free-electron model shown by the solid line, where the value of the redshift, in a range between 127 eV and 153 eV, is close to the binding energy of the 1s state of Be atom. This indicates that a bound electron can provide a redshift comparable to its binding energy.

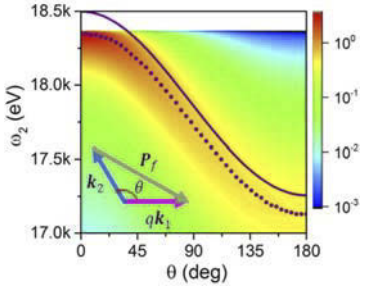

Fig. 5. The integral of $|\Phi_i(\mathbf{P}_f + \mathbf{k}_2 + (u_p - q)\mathbf{k}_1)|^2$ over $\mathbf{P}_f$ as a function of ω_2 and θ. The dots denote the scattered photon energy corresponding to the peaks at different scattering angles and the solid line represents the prediction by Eq. (21).

Next, by analyzing other terms in Eq. (22)-(23), we find that the shifts of the peak positions of the DDP spectra can also be affected by the value of the final electron momentum besides the binding energy of the electron. Specifically, for EMM transition, the T-matrix element depends linearly on the value of the electron momentum P_f. According to the energy conservation, P_f

Optics EXPRESS

decreases with the increase of the scattered photon energy, such that the peak positions of the DDP determined by EMM transition are always red shifted to the prediction of the free-electron model. On the contrary, for LEM transition, with the variation of the scattering angle, the dependence of the T-matrix element on the value of the electron momentum P_f is nonmonotonic, resulting in the non-unidirectional shift of the peak position (may red shift or blue shift).

To illustrate the DDP spectra more comprehensively, the total DDP, the DDP due to EEM and LEM transitions as a function of the scattering angle and the scattered photon energy at different azimuthal angles are calculated and shown at the top, middle and bottom of Fig. 6, respectively. The dots show the peak positions of the total DDP spectra and the solid lines predict the scattered photon energy by the free-electron model. Firstly, for $\phi = 0°$, one may find that, the peak positions are below the energy predicted by the free-electron model at θ<90°, while the peak position jumps above the prediction of the free-electron model at $\theta = 90°$, and keeps blue shifted until θ>94°. These results can be explained as follows: (1) At $\theta = 90°$, the total DDP is determined by LEM transition, since EMM transition and the cross term are both zero due to $\boldsymbol{\epsilon}_1 \cdot \boldsymbol{\epsilon}_2^* = 0$, where $\mathbf{k}_2 \perp \mathbf{k}_1$ and $\mathbf{k}_2 \parallel \boldsymbol{\epsilon}_1$ causes $\boldsymbol{\epsilon}_2 \perp \boldsymbol{\epsilon}_1$. Therefore, the DDP spectrum changing from redshift to blueshift is due to the contribution of the LEM transition which is blue shifted at $\theta = 90°$; (2) For $\theta \in 90° \pm 4°$ except 90°, the cross term begins to play a role in the contribution to DDP, as shown in Fig. 3(a) and (b), hence the peak position of the DDP spectrum

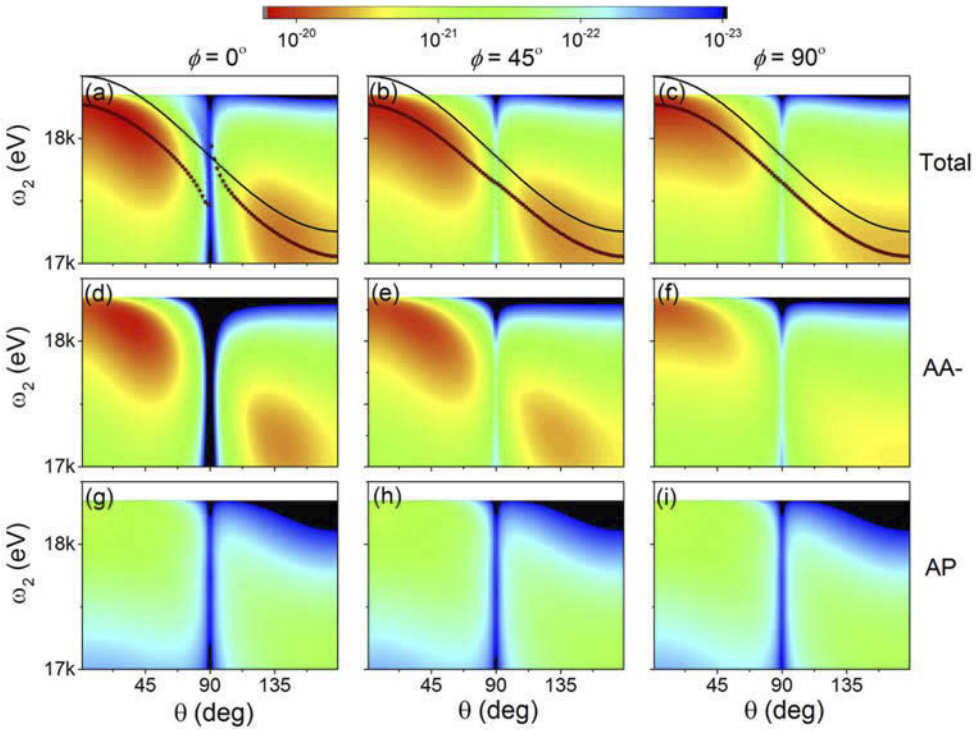

Fig. 6. Angle-resolved energy spectra of two-photon NCS by Be. The DDP is shown as a function of the scattering angle θ and the scattered photon energy ω_2 at different azimuthal angles $\phi = 0°$ (left column), $\phi = 45°$ (middle column) and $\phi = 90°$ (right column). The total DDP, the DDP due to EMM, and the DDP due to LEM are shown in (**a**)-(**c**), (**d**)-(**f**) and (**g**)-(**i**), respectively. The solid lines represent ω_2 determined by the free-electron model Eq. (21) and the dots denote the peak positions of the total DDP. The laser parameters are the same as Fig. 3.

Optics EXPRESS

changes to redshift for θ<90° and to blueshift for θ>90°; (3) For the angles θ<86° or θ>94°, EMM transition dominates the contribution to the total DDP, hence the peak position of the total DDP is redshifted to the energy predicted by the free-electron model.

Secondly, for $\phi = 45°$ and 90°, it shows that the peak positions of total DDP spectra are always redshifted to the energy predicted by the free-electron model. By comparing the DDP spectra contributed by EMM (Fig. 6(d)-(f)) with those contributed by LEM (Fig. 6(g)-(i)), one can find that the total DDP is dominated by the contribution from EMM transition. Owing to the fact that the peak positions of the DDP of EMM transition are always redshifted, the peak positions of total DDP will also red shift to the prediction of the free-electron model when EMM transition is dominant.

We now qualitatively compare our NCS spectra with the experimental results [22] by using a magnification factor δ. The DDP of two-photon NCS is shown in Fig. 7 at $\theta = 89°$ with $\delta = 2\times10^{16}$ (a), $\theta = 103°$ with $\delta = 3.5\times10^{14}$ (b), $\theta = 117°$ with $\delta = 1.1\times10^{14}$ (c) and $\theta = 131°$ with $\delta = 7.3\times10^{13}$. In Fig. 7, the curves and geometric symbols represent, respectively, the theoretical and experimental results under various laser intensities. The consistency between the theoretical and experimental results is reflected in the following two points: First, the peak positions in the experiment and our theory are both red shifted to the predicted value of free-electron model. Second, the dependence of the DDP spectra on the X-ray laser intensity in our theory is the same as that of the experiment. Especially, in our method, the second-order nonlinear effects of the laser intensity can be found in the expression of the T-matrix elements of LEM and EMM, i.e., the term $\mathcal{J}_q(\zeta,\eta)$ in T_{AP} and the term $\Lambda\mathcal{J}_{q-1}(\zeta,\eta)$ in T_{AA-} are proportional to the laser intensity. For the discrepancies between theoretical and experimental results, one may notice that the experimental spectra are wider than the theoretical spectra, this is probably because the laser in the experiment cannot be monochromatic and have a certain spectral width,

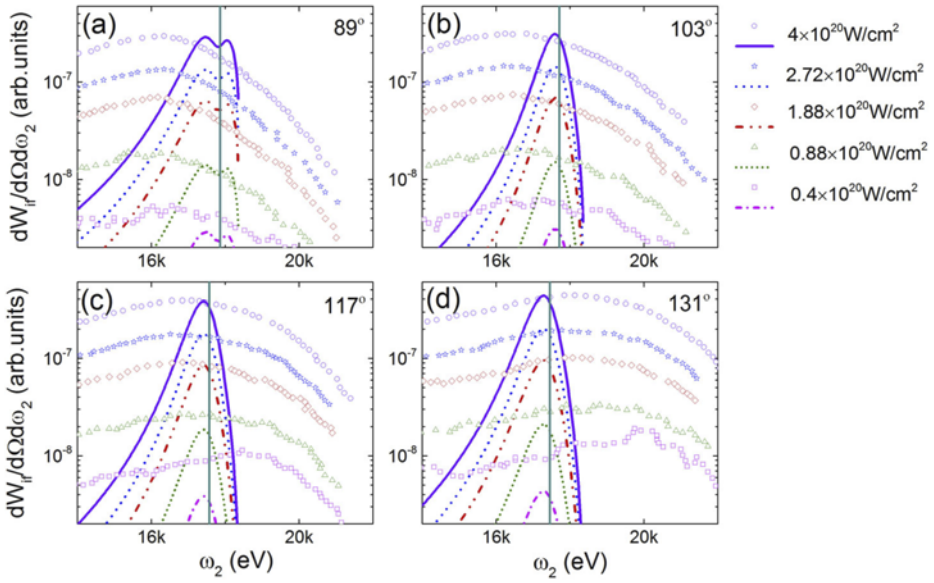

Fig. 7. Comparison between the DDP of theory and experiment. The DDP for two-photon NCS by Be at $\theta = 89°$ (**a**), $\theta = 103°$ (**b**), $\theta = 117°$ (**c**) and $\theta = 131°$ (**d**). The curves and geometric figures represent, respectively, the theoretical and experimental values under different laser intensities. The incident photon energy ω_1=9.25 keV. The azimuthal angle of the wave vector of scattered light is same to Fig. 3. Note: the theoretical values in the same graph are magnified by the same magnification factor.

Optics EXPRESS

but the spectral width is not considered in our theoretical calculation. On the other hand, the 1-mm-thick Be target is used in the experiments, while we only consider the interaction between the X-ray laser and a Be atom in our calculation, this may also induce some differences.

4. Conclusion

We have extended the frequency-domain theory to investigate the NCS of two X-ray photons by an atom. Our theoretical results are in qualitative agreement with the experimental results of Ref. [22]. By analyzing the EMM and LEM transition matrix elements, we find that the redshift in the DDP spectra of the NCS process can be attributed to the atomic binding potential and the momentum transfer from the incident photons to the electron during the collision. Our results have demonstrated that the redshift can be observed in both forward and backward directions. All these findings promote significantly the understanding of the nonlinear scattering processes of bound electrons in X-ray laser fields.

Funding. National Natural Science Foundation of China (11774411, 11834015, 12074418).

Acknowledgments. We thank all the members of SFAMP club for helpful discussions. S.S thanks D. Krebs and M. Fuchs for helpful discussions.

Disclosures. The authors declare no conflicts of interest.

Data availability. Data underlying the results presented in this paper are not publicly available at this time but may be obtained from the authors upon reasonable request.

References

1. A. H. Compton, "A quantum theory of the scattering of x-rays by light elements," Phys. Rev. **21**(5), 483–502 (1923).
2. J. W. Du Mond, "Compton modified line structure and its relation to the electron theory of solid bodies," Phys. Rev. **33**(5), 643–658 (1929).
3. J. W. DuMond, "The linear momenta of electrons in atoms and in solid bodies as revealed by x-ray scattering," Rev. Mod. Phys. **5**(1), 1–33 (1933).
4. M. Cooper, "Compton scattering and electron momentum distributions," Adv. Phys. **20**(86), 453–491 (1971).
5. W. Ching and J. Callaway, "Band structure, cohesive energy, optical conductivity, and compton profile of lithium," Phys. Rev. B **9**(12), 5115–5121 (1974).
6. D. Laurent, C. Wang, and J. Callaway, "Energy bands, compton profile, and optical conductivity of vanadium," Phys. Rev. B **17**(2), 455–461 (1978).
7. P. Jaiswal and A. Shukla, "Kinetically balanced gaussian basis-set approach to relativistic compton profiles of atoms," Phys. Rev. A **75**(2), 022504 (2007).
8. P. Eisenberger and P. Platzman, "Compton scattering of x rays from bound electrons," Phys. Rev. A **2**(2), 415–423 (1970).
9. R. Ribberfors, "Relationship of the relativistic compton cross section to the momentum distribution of bound electron states," Phys. Rev. B **12**(6), 2067–2074 (1975).
10. V. Florescu and R. Pratt, "K-shell compton scattering at high photon energy," Phys. Rev. A **80**(3), 033421 (2009).
11. L. LaJohn, "Low-momentum-transfer nonrelativistic limit of the relativistic impulse approximation expression for compton-scattering doubly differential cross sections and characterization of their relativistic contributions," Phys. Rev. A **81**(4), 043404 (2010).
12. R. Pratt, L. LaJohn, V. Florescu, T. Surić, B. K. Chatterjee, and S. Roy, "Compton scattering revisited," Radiat. Phys. Chem. **79**(2), 124–131 (2010).
13. P. Emma, R. Akre, J. Arthur, R. Bionta, C. Bostedt, J. Bozek, A. Brachmann, P. Bucksbaum, R. Coffee, F.-J. Decker, Y. Ding, D. Dowell, S. Edstrom, A. Fisher, J. Frisch, S. Gilevich, J. Hastings, G. Hays, P. Hering, Z. Huang, R. Iverson, H. Loos, M. Messerschmidt, A. Miahnahri, S. Moeller, H.-D. Nuhn, G. Pile, D. Ratner, J. Rzepiela, D. Schultz, T. Smith, P. Stefan, H. Tompkins, J. Turner, J. Welch, W. White, J. Wu, G. Yocky, and J. Galayda, "First lasing and operation of an ångstrom-wavelength free-electron laser," Nat. Photonics **4**(9), 641–647 (2010).
14. R. Mitzner, B. Siemer, M. Neeb, T. Noll, F. Siewert, S. Roling, M. Rutkowski, A. Sorokin, M. Richter, P. Juranic, K. Tiedtke, J. Feldhaus, W. Eberhardt, and H. Zacharias, "Spatio-temporal coherence of free electron laser pulses in the soft x-ray regime," Opt. Express **16**(24), 19909–19919 (2008).
15. B. W. McNeil and N. R. Thompson, "X-ray free-electron lasers," Nat. Photonics **4**(12), 814–821 (2010).
16. J. N. Galayda, J. Arthur, D. F. Ratner, and W. E. White, "X-ray free-electron lasers-present and future capabilities," J. Opt. Soc. Am. B **27**(11), B106–B118 (2010).
17. P. R. Ribic and G. Margaritondo, "Status and prospects of x-ray free-electron lasers (x-fels): a simple presentation," J. Phys. D: Appl. Phys. **45**(21), 213001 (2012).
18. S. Shwartz, M. Fuchs, J. Hastings, Y. Inubushi, T. Ishikawa, T. Katayama, D. Reis, T. Sato, K. Tono, M. Yabashi, S. Yudovich, and S. Harris, "X-ray second harmonic generation," Phys. Rev. Lett. **112**(16), 163901 (2014).

Optics EXPRESS

19. K. Tamasaku, E. Shigemasa, Y. Inubushi, T. Katayama, K. Sawada, H. Yumoto, H. Ohashi, H. Mimura, M. Yabashi, K. Yamauchi, and T. Ishikawa, "X-ray two-photon absorption competing against single and sequential multiphoton processes," Nat. Photonics **8**(4), 313–316 (2014).
20. S. Ghimire, M. Fuchs, J. Hastings, S. C. Herrmann, Y. Inubushi, J. Pines, S. Shwartz, M. Yabashi, and D. A. Reis, "Nonsequential two-photon absorption from the k shell in solid zirconium," Phys. Rev. A **94**(4), 043418 (2016).
21. L. Young, E. P. Kanter, B. Kraessig, Y. Li, A. March, S. Pratt, R. Santra, S. Southworth, N. Rohringer, L. DiMauro, G. Doumy, C. Roedig, N. Berrah, L. Fang, M. Hoener, P. Bucksbaum, J. Cryan, S. Ghimire, J. Glownia, D. Reis, J. Bozek, C. Bostedt, and M. Messerschmidt, "Femtosecond electronic response of atoms to ultra-intense x-rays," Nature (London) **466**(7302), 56–61 (2010).
22. M. Fuchs, M. Trigo, J. Chen, S. Ghimire, S. Shwartz, M. Kozina, M. Jiang, T. Henighan, C. Bray, G. Ndabashimiye, P. H. Bucksbaum, Y. Feng, S. Herrmann, G. A. Carini, J. Pines, P. Hart, C. Kenney, S. Guillet, S. Boutet, G. J. Williams, M. Messerschmidt, M. M. Seibert, S. Moeller, J. B. Hastings, and D. A. Reis, "Anomalous nonlinear x-ray compton scattering," Nat. Phys. **11**(11), 964–970 (2015).
23. A. N. Hopersky, A. M. Nadolinsky, and S. A. Novikov, "Compton scattering of two x-ray photons by an atom," Phys. Rev. A **92**(5), 052709 (2015).
24. D. Krebs, D. A. Reis, and R. Santra, "Time-dependent qed approach to x-ray nonlinear compton scattering," Phys. Rev. A **99**(2), 022120 (2019).
25. A. Venkatesh and F. Robicheaux, "Simulation of nonlinear compton scattering from bound electrons," Phys. Rev. A **101**(1), 013409 (2020).
26. D.-S. Guo, T. Åberg, and B. Crasemann, "Scattering theory of multiphoton ionization in strong fields," Phys. Rev. A **40**(9), 4997–5005 (1989).
27. L. Gao, X. Li, P. Fu, R. Freeman, and D.-S. Guo, "Nonperturbative quantum electrodynamics theory of high-order harmonic generation," Phys. Rev. A **61**(6), 063407 (2000).
28. B. Wang, L. Gao, X. Li, D.-S. Guo, and P. Fu, "Frequency-domain theory of high-order above-threshold ionization based on nonperturbative quantum electrodynamics," Phys. Rev. A **75**(6), 063419 (2007).
29. B. Wang, Y. Guo, J. Chen, Z.-C. Yan, and P. Fu, "Frequency-domain theory of nonsequential double ionization in intense laser fields based on nonperturbative qed," Phys. Rev. A **85**(2), 023402 (2012).
30. M. Gell-Mann and M. Goldberger, "The formal theory of scattering," Phys. Rev. **91**(2), 398–408 (1953).
31. T. Åberg, D.-S. Guo, J. Ruscheinski, and B. Crasemann, "Scattering-theoretical approaches to multiphoton ionization in strong fields," Phys. Rev. A **44**(5), 3169–3178 (1991).
32. T. Åberg, "Quantum electrodynamics of multiphoton ionization," Phys. Scr. **1993**, 173 (1993).
33. D.-S. Guo and G. W. Drake, "Stationary solutions for an electron in an intense laser field. i. single-mode case," J. Phys. A: Math. Gen. **25**(11), 3383–3397 (1992).
34. D.-S. Guo and G. W. Drake, "Stationary solutions for an electron in an intense laser field. ii. multimode case," J. Phys. A: Math. Gen. **25**(20), 5377–5394 (1992).
35. L. S. Brown and T. Kibble, "Interaction of intense laser beams with electrons," Phys. Rev. **133**(3A), A705–A719 (1964).